

Article

Highly Hydrophobic Organic Coatings Based on Organopolysilazanes and Silica Nanoparticles: Evaluation of Environmental Degradation

Lucía Pérez-Gandarillas , Daniel Aragón, Carmen Manteca, Marina Gonzalez-Barriuso , Laura Soriano, Abraham Casas  and Angel Yedra

Centro Tecnológico de Componentes-CTC, Scientific and Technological Park of Cantabria (PCTCAN),
39011 Santander, Spain

* Correspondence: lperez@centrotecnologicocctc.com

Abstract: Hydrophobic coatings have potential applications in various fields, including for corrosion and weathering protection. In this study, we investigated the use of organopolysilazanes (OPSZs) combined with hydrophobic nanoparticles (NPs) on steel as a substrate to obtain hydrophobic coatings. The coatings were characterized using various techniques, and their hydrophobic properties and corrosion and weathering resistance were evaluated under near-shore marine conditions with high salinity, humidity and UV radiation. Our results show that the coatings exhibited excellent hydrophobic properties and significantly improved corrosion and weathering resistance compared to an uncoated steel and a pristine polymer. These findings suggest that the developed coatings have the potential to provide protection against corrosion for atmospheric and splash exposures in marine environments.

Keywords: hydrophobicity; hydrophobic coatings; organopolysilazanes; hydrophobic nanoparticles; corrosion resistance; environmental degradation



Citation: Pérez-Gandarillas, L.; Aragón, D.; Manteca, C.; Gonzalez-Barriuso, M.; Soriano, L.; Casas, A.; Yedra, A. Highly Hydrophobic Organic Coatings Based on Organopolysilazanes and Silica Nanoparticles: Evaluation of Environmental Degradation. *Coatings* **2023**, *13*, 537. <https://doi.org/10.3390/coatings13030537>

Academic Editor: Ioannis Karapanagiotis

Received: 23 January 2023

Revised: 22 February 2023

Accepted: 22 February 2023

Published: 1 March 2023



Copyright: © 2023 by the authors. Licensee MDPI, Basel, Switzerland. This article is an open access article distributed under the terms and conditions of the Creative Commons Attribution (CC BY) license (<https://creativecommons.org/licenses/by/4.0/>).

1. Introduction

Surface wetting behavior can generally be classified into four different regimes based on the value of the water contact angle (WCA, θ): superhydrophilic ($\theta < 10^\circ$), hydrophilic ($10^\circ < \theta < 90^\circ$), hydrophobic ($90^\circ < \theta < 150^\circ$), and superhydrophobic ($\theta > 150^\circ$) regimes [1,2]. Studies have demonstrated that an adequate combination of surface roughness and chemical composition is the key for the preparation of hydrophobic and superhydrophobic engineered surfaces.

Hydrophobic and superhydrophobic surfaces have aroused great attention among the scientific and industrial communities for their high water repellence, which entails associated properties of interest, such as anti-corrosion, self-cleaning, anti-icing, anti-adherence, reduction of bio-fouling, and antimicrobial or water vapor barrier effects, among others [1,2]. Therefore, these surfaces offer a wide range of technological applications for diverse sectors.

Various materials and techniques have been used to prepare hydrophobic and superhydrophobic coatings, including both organic and inorganic materials, as well as diverse techniques, such as electrochemical deposition [3], sol-gel [4,5], plasma etching [6], chemical vapor deposition [7], templating, etching, anodization, self-assembling, dip-coating and spray-coating techniques [8–10]. These methods can result in different morphologies, roughnesses, and chemical compositions of the coatings, which impact their water-repellent properties [10]. However, the main limitation of most of the employed methods is their high cost, associated with their application complexity or the amount of processing required to accurately create nanostructures. In addition, since hydrophobicity is a superficial property, the main disadvantage is its limited durability against degradation by external agents.

Hydrophobic surfaces can be deteriorated by several environmental mechanisms, mainly by mechanical wear, although others, such as chemical reactions with solvents or gases, ultraviolet (UV) exposure, rain, humidity and contamination, also contribute [11].

The vast majority of hydrophobic and superhydrophobic surfaces have a very limited resistance to abrasion and environmental degradation (losing hydrophobicity at the outermost layer), and, therefore, the stability of the nanocoating has a reduced durability [1,12]. The challenge of durability has restricted the use of hydrophobic surfaces in commercial and industrial applications [11].

In order to overcome the aforementioned limitations, the use of nanotechnology for the formulation of new durable and effective hydrophobic coatings is postulated as a potential solution. Polymer-based nanocomposites are one of the most popular fields of current research. Specifically, nanocomposite fabrication from organic polymers using nanoparticles as additives has been creating high expectations in the coatings industry sector [13].

Organic nanocomposite coatings consist of a polymeric matrix to which a nanofiller is integrated, which provides the intended functionality to the surface. The great advantages of organic coatings over other types of coatings are the abilities to obtain excellent properties at a lower cost and to use simple application technologies.

However, due to the high specific surface of nanomaterials, the tendency to aggregate means that their integration into polymeric matrices is still a technically complex process. In this sense, in order to achieve the characteristic of hydrophobicity and, at the same time, durability over time, it is necessary to guarantee an optimal integration of the nanomaterials in the polymeric matrix.

Different authors have carried out studies to obtain hydrophobic paints based on nanotechnology [14–16]. Unfortunately, in general, the polymeric matrices surround the integrated hydrophobic nanoparticles, inhibiting their hydrophobic character (Figure 1a). Therefore, improving nanoparticle–polymer and coating–substrate interfacial adhesions may be the key to improving the durability of hydrophobic coatings. The use of a polymer as an anchor binder that acts as a film-forming agent can (i) avoid the inhibition of the hydrophobic functionality of nanoparticles and (ii) ensure the adhesion of nanoparticles to the substrate (Figure 1b).

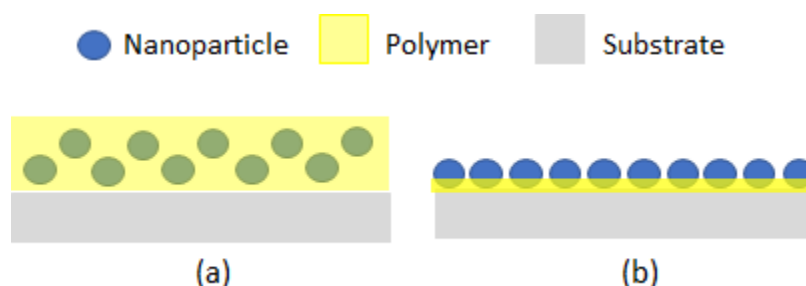


Figure 1. Schematic illustration of nanoparticle integration: (a) complete embedment of nanoparticles in the polymer; (b) polymer acting as bonding layer between nanoparticles and substrate.

The scientific community is searching for high-strength polymeric matrices, and, in this context, polysilazanes are attracting attention due to their extraordinary properties [17]. Polysilazanes (PSZs) are a class of special polymers with a structure containing alternating nitrogen and silicon atoms: $-(SiR^1R^2-NR^3)_n-$. These polymers can be converted to ceramics at approximately 1000 °C and have been widely used as precursors for silicon carbonitrides [18–20].

In particular, organopolysilazanes (OPSZs) are PSZs that bond to carbon atoms. The high reactivities of the Si-H and N-H groups present in the structures of OPSZs form a very dense silica network, notably improving adherence to different substrates (glass, plastic, metal, etc.) [21]. OPSZs are highly crosslinked, combine good barrier properties

and exhibit a high mechanical strength and a strong affinity with metallic substrates. In addition, recently, OPSZs have been developed to rapidly cure at room temperature by interacting with ambient moisture, which has generated considerable interest in simplifying the curing process. These types of polymers are used in various sectors for high-value-added applications, such as electronics. In terms of corrosion resistance, their good barrier properties have been proven [21–23].

There are studies in the scientific literature that use this type of polymer for hydrophobicity applications [24,25]. However, research in this field has shown that the hydrophobicity values achieved using organopolysilazanes (in the range between a 90° and 95° water contact angle) are far from those of superhydrophobicity. In most of the studies carried out, the OPSZ is applied pure mainly on aluminum due to its adhesion capacity, which prevails over hydrophobicity [26]. Therefore, there is scarce literature on its use on other substrates with greater application, such as steel [21,27].

The objective of this work is to study the application of OPSZ combined with hydrophobic nanoparticles on steel as a substrate to obtain highly hydrophobic coatings. Once hydrophobicity is achieved, the durability is tested under near-shore marine conditions with high salinity, humidity and UV radiation. This test allows for the evaluation of how the hydrophobic property favors the corrosion resistance of a coating.

2. Materials and Methods

2.1. Materials

A commercially available OPSZ (Durazane 1500 Rapid Cure) was supplied by Merck KGaA (Darmstadt, Germany). This polysilazane is a low-viscosity liquid, with a high crosslink density and rapid moisture curing at room temperature. As hydrophobic nanoparticles, commercial fumed silica powder, surface-treated with polydimethylsiloxane (Aerosil R202, Evonik Industries AG, Essen, Germany), was used. As solvents, butyl acetate (BAC) and acetone were employed.

For the selection of the solvent and the optimization of the NP percentage, glass substrates were used (76 mm × 26 mm × 1 mm). For the degradation evaluation, standard samples of low-carbon steel (F 6702 according to UNE-36086-1) from Espancolor (Barcelona, Spain) were used as substrates (150 mm × 75 mm × 0.8 mm).

2.2. Methods

2.2.1. Nanoparticle Integration

In order to provide the hydrophobic functionality to the coating, different amounts of nanoparticles were mixed with the OPSZ polymer. Firstly, the hydrophobic silica nanoparticles were dispersed in the solvent by using ultrasound for 15 min (Sonopuls HD3200, Bandelin, Berlin, Germany). To this solution, different amounts of OPSZs were added, and the nanoparticles were integrated via mechanical stirring into the polymer in a range between 0% and 50% of the mass of the polymer. The OPSZ worked as a binder to anchor the nanoparticles to the substrate.

2.2.2. Sample Preparation

For the deposition of the coatings on steel substrates, two different techniques were used in order to compare their effects on the final properties of the coating. On the one hand, spray-coating deposition was carried out using a compressed dry air spray gun (Mini Xtreme, Sagola, Vitoria, Spain), operating at a pressure of 2 bars. The spray technique has the advantages of being able to carry out coatings both on a large scale and of irregular parts and at a low price. On the other hand, the dip-coating technique is adequate for the synthesis of thin layers, has the advantage of simplicity and the possibility of adjusting the parameters to obtain more precise coatings. According to our own expertise, the following conditions of the dip coater (ND-DC 11/1, Nadetech Innovations, Noain, Spain) were selected: 100 mm/min for the immersion rate and 30 mm/min for the emersion rate.

A preliminary evaluation of the formulations with different percentages of NPs was carried out by depositing the coatings on glass substrates via dip coating. Then, an optimum formulation was chosen in terms of hydrophobicity and color variation. With this formulation, steel substrates were coated using both the spray- and dip-coating methods (Figure 2).

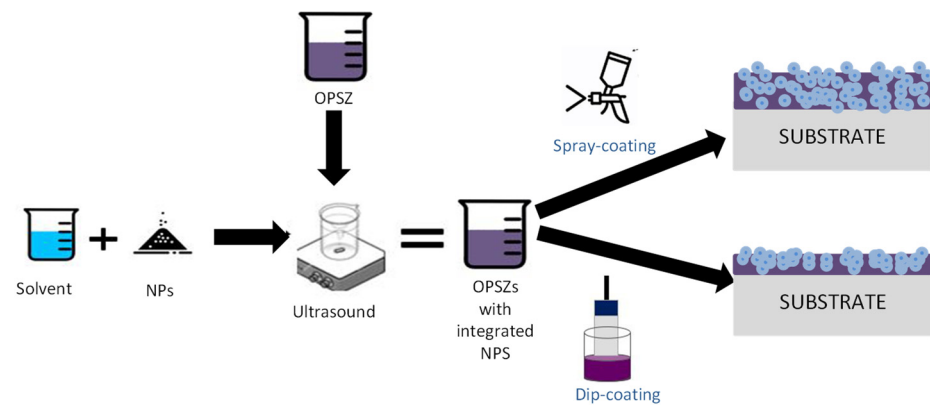
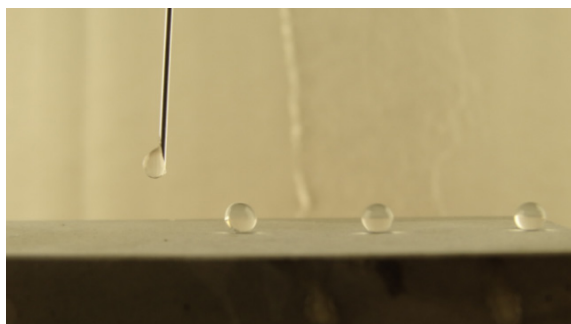


Figure 2. Scheme of the sample preparation process.

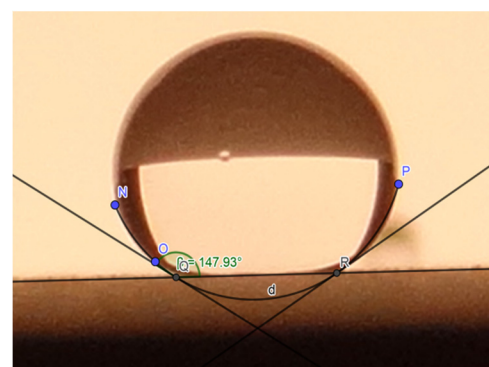
Prior to the deposition processes, the steel substrates were washed with ethanol to remove the protective grease. The samples were cured at room temperature for 24 h ($T = 20\text{--}25\text{ }^{\circ}\text{C}$; relative humidity = 40%–50%).

2.2.3. Water Contact Angle

The water contact angle (WCA) is a parameter that discriminates the hydrophobic properties of a surface. The contact angle is measured as the angle formed by the line of the surface with the line tangent to the intersections of the modified circumference of a drop. To perform this measurement, an experimental device was prepared consisting of a flat horizontal surface, on which the painted specimen was supported, and a camera was supported on a tripod so that the focus was centered at the same height as the surface of the specimen. Pictures were taken of the water droplets on the substrate and analyzed with the mathematical software GeoGebra [28] to obtain the contact angle (Figure 3). The WCA measurements were performed in triplicate, taking the average and standard deviation of such measurements.



(a)



(b)

Figure 3. (a) Water drops rolling off (b) Water contact angle measurement.

2.2.4. Coating Thickness

To measure the coating thickness, a portable electronic Positector 6000 (DeFekco, Ogdensburg, NY, USA) was used. The measurements made by this equipment are fast and non-destructive since it uses magnetic principles and Foucault's current to measure the thickness of the paint on ferrous and non-ferrous metals.

2.2.5. Color Variation

A portable spectrophotometer (X-Rite, model RM200QC, Grand Rapids, MI, USA) was used to evaluate the color variation of the coating with respect to the substrate. This equipment can measure the opacity and transparency of a coating through color variation (ΔE). ΔE can be determined from the L^*a^*b color space, also referred to as CIELAB, according to Equation (1):

$$\Delta E = \sqrt{\Delta L^2 + \Delta a^2 + \Delta b^2} \quad (1)$$

where L refers to lightness, a represents red to green coordinates, and b represents coordinates from blue to yellow.

Therefore, ΔE is the numerical comparison between two color samples and indicates the differences in absolute color coordinates. Likewise, the color variation allows for an evaluation of the coating after the degradation tests. According to the literature, if $\Delta E < 5$, color variations are negligible [29]. Color variation was measured in triplicate, taking the average and standard deviation of such measurements.

2.2.6. Environmental Degradation Tests

The specimens obtained were subjected to different degradation tests in order to evaluate their durability.

The corrosion resistance was evaluated through a salt spray test. This test is generally suitable for testing corrosion protection as a quick analysis of discontinuities, pores and damage in organic and inorganic coatings. The salt spray test consists of spraying a sodium chloride solution (5% NaCl) in a controlled environment inside a salt spray chamber (Dycometal, model SSC400, Barcelona, Spain) where the specimens are located. To carry out this test, the ISO 9227:2017 standard was taken as a reference. Two 24 h cycles were carried out (total time = 48 h) in this work.

The coatings were also exposed to artificial weathering (fluorescent UV lamps and water) with the purpose of simulating the natural aging processes caused by environmental agents, such as sunlight and rain. This test consists of introducing the test pieces into a QUV chamber (Q-Lab, Westlake, OH, USA), where they are exposed to alternating cycles of UV light, condensation and high temperatures, simulating the damage caused by sunlight, rain and dew. This test was carried out, taking the ISO 11507:2007 standard as a reference, during a 120 h cycle with alternate cycles of sprayed water and UV light and an inspection every 24 h.

The resistance of the coatings to environmental degradation was evaluated by measuring the contact angle and color variation before and after the degradation tests (Figure 4).

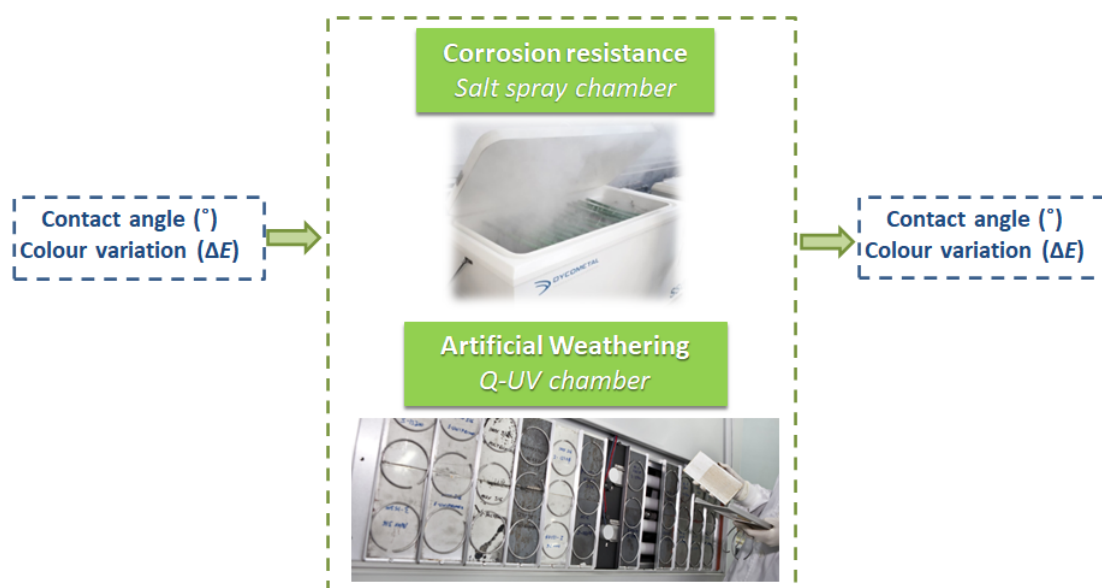


Figure 4. Environmental degradation tests conducted to evaluate the durability of coatings.

2.2.7. Electrochemical Impedance Spectroscopy (EIS)

Electrochemical Impedance Spectroscopy (EIS) measurements were performed on the developed samples. EIS is an electrochemical technique usually utilized for evaluating the corrosion behavior of coatings and provides insights into the corrosion reaction of a substrate [30]. An evaluation of the impedance of a coated system as a function of frequency supplies useful information regarding the barrier properties of the coating, the corrosion susceptibility of the substrate and the interfacial layer [31].

EIS tests were performed on an Autolab PGSTAT204N potentiostat, (Metrohm Hispania, Madrid, Spain) with the Nova 2.1 software version for analyses. A three-electrode corrosion cell was used with the coated samples as a working electrode, a platinum wire as a counter electrode, a Ag/AgCl (3.5 M KCl) as a reference electrode and the samples being tested as working electrodes. A 5 wt% sodium chloride solution in deionized water was used as the electrolyte. The coating exposure area for testing was 12.6 cm², corresponding to a circular area of 4 cm in diameter. The tests were conducted under stagnant conditions at room temperature (20–25 °C) and were performed on two coated replicas per system inside a Faraday cage. For this study, the sweep conditions for running the EIS tests were carried out over a frequency range from 100 kHz to 0.01 Hz with 7 readings per decade of frequency at 20 mVRMS amplitude sinusoidal perturbation with respect to the open-circuit potential.

3. Results and Discussion

3.1. Selection of Solvent

In order to use the minimum amount of nanoparticles necessary to achieve hydrophobicity, it is necessary to first dilute polysilazane in a solvent. The selection of a proper solvent for polymer dissolution is important to guarantee good nanoparticle dispersion and the durability of the coating. According to the technical datasheet, the Durazane 1500 Rapid Cure Resin reacts in the presence of water, steam or alcohols, so it is important to use solvents with the lowest possible water content. Organic solvents, such as alkanes, esters, ethers, aromatics and ketones, are chemically compatible with the resin. After consultation with the polymer manufacturer, two potential solvents were selected based on their availability/price ratio: butyl acetate (BAC) and acetone.

For the evaluation of which of the two solvents works better, different solutions with different percentages of OPSZs were prepared via mechanical stirring using each type of solvent (BAC and acetone).

It was found that, in both cases, the viscosity was lower than that of the original polymer and that there was no problem in spray painting or dip coating. However, color degradation (yellowing) over time was observed in the formulations where acetone was used. Therefore, BAC was selected for the development of the formulations.

3.2. Evaluation of Optimum Percentage of Nanoparticles

Different ratios of OPSZ:NPs (the percentage of NPS varied from 0% to 50%) were used and deposited in glass samples via dip coating (Figure 5). It can be observed that, when the percentage of NPs in the formulation increases, the coating becomes whiter and opaquer.

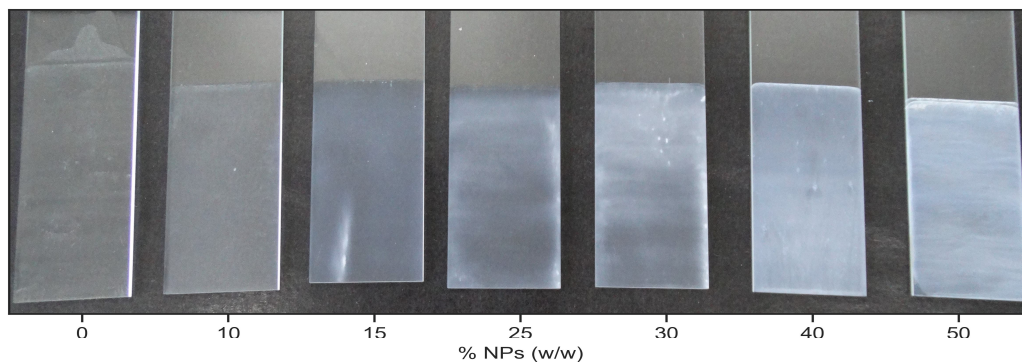


Figure 5. Glass samples coated with several ratios of OPSZ/NPs.

Then, the WCA and the color variation were measured in these samples and are presented in Figures 6 and 7.

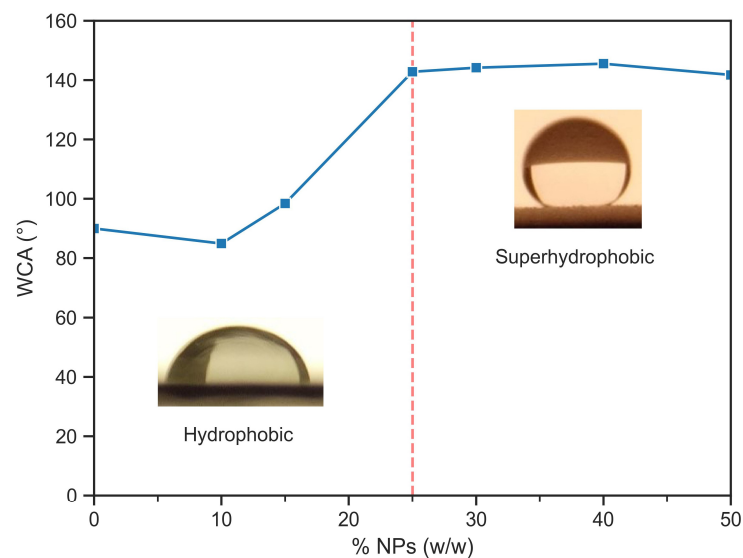


Figure 6. WCA in a flat surface for different concentrations of NPs.

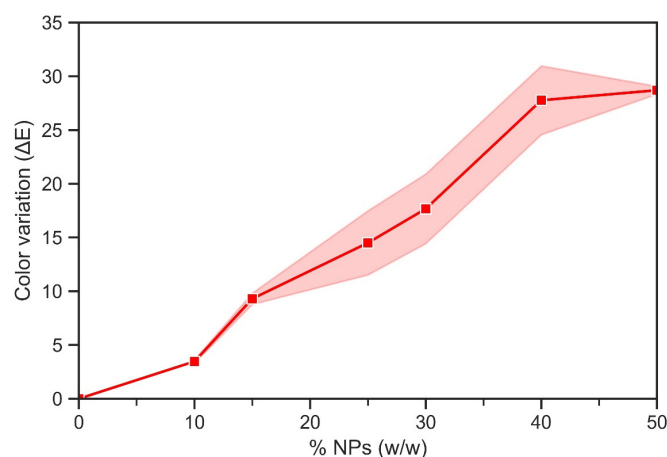


Figure 7. Color variation (ΔE) for different concentrations of NPs (shadowed area corresponds to the standard deviation).

The data presented in Figure 6 clearly illustrate a correlation between the WCA and the NP content. As shown, the maximum WCA is achieved when the NP content is increased up to 25%. Beyond this point, the WCA remains constant. The resulting WCA indicates a highly hydrophobic behavior, very close to the superhydrophobic regime.

The correlation between the WCA and nanoparticle concentration has already been observed by other authors [32–35]. It could be explained by the Cassie–Baxter model because a suitable and optimal hydrophobic NP integration into resin promotes the formation of a micro- and nano-roughness surface, where air trapping takes place [1,11]. These air pockets significantly increase hydrophobicity.

Regarding the color variation, it increases when the percentage of NPs in the formulation increases. It is obvious that the NPs contribute to the changing color of the polymers, because they act like white pigments.

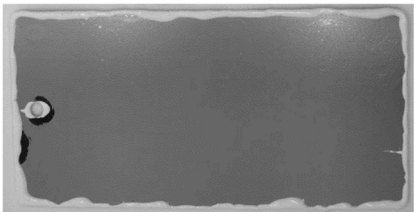
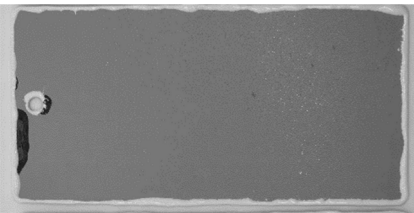
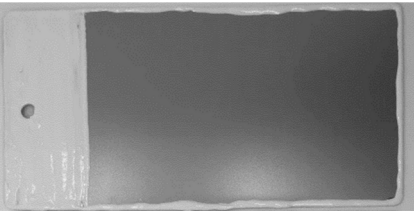
According to the WCA results, the chosen proportion of OPSZ:NPs is 75:25. With this ratio, hydrophobicity is achieved, while the color variation is maintained as minimum as possible. With higher percentages of NPs, hydrophobicity is not improved, while the coatings become whiter.

Therefore, with a 75:25 proportion of OPSZ:NPs, a bench test of the samples is carried out using the spray- and dip-coating techniques. The main characteristics of the obtained samples are shown in Table 1.

As can be seen in the pictures included in Table 1, the samples obtained via dip coating are more homogeneous than the ones obtained via spraying, and the thickness is much lower. Moreover, the dip-coated samples have less color variation than the sprayed samples. This is directly related to the reduced thickness (5 μm) that is obtained via dip coating. A lower thickness implies less color variation.

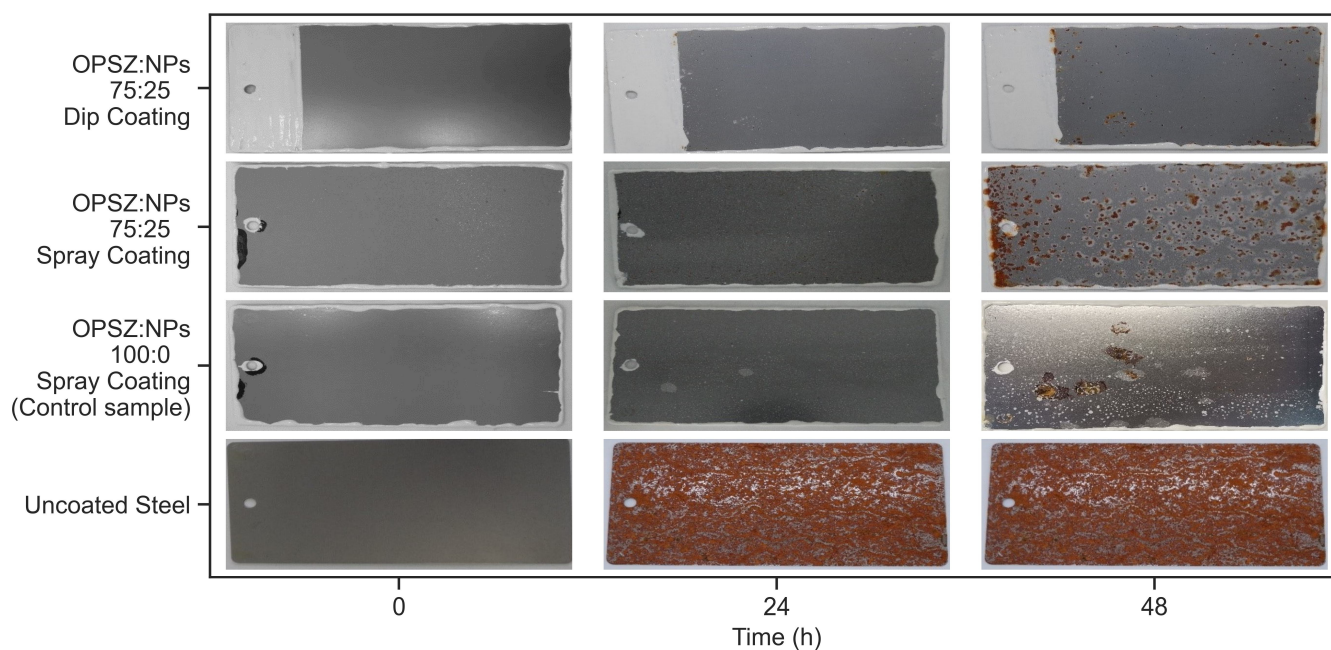
It can also be observed that the quality of the sprayed coating is not good and that surface defects appear on the surface. These surface defects are attributed to the deposition method. During the spraying process, a rapid evaporation of the solvent takes place, and, therefore, the nanoparticles are not wet enough when reaching the substrate surface. The Si-N bonds present in the polysilazane structure react with the moisture present in the air without being deposited on the substrate, thus producing cyclotetrasiloxanes [36], which are solid at room temperature.

Table 1. Main characteristics of the studied coatings.

Formulation	Thickness (μm)	ΔE	WCA ($^\circ$)	Appearance (Dimensions $150 \times 75 \text{ mm}$)
OPSZ:NPs 100:0 (control sample obtained via spray coating)	29 ± 1	-	90 ± 2	
OPSZ:NPs 75:25 Spray coating	63 ± 10	17 ± 1	147 ± 1	
OPSZ:NPs 75:25 Dip coating	5 ± 1	9 ± 1	147 ± 1	

3.3. Salt Spray Test Results

The salt spray test lasted a total of 48 h, although a visual inspection and measurements of the WCA were also carried out after the first 24 h. The pictures taken during the test are included in Figure 8, while Figure 9 shows the evolution of the WCA.

**Figure 8.** Evolution of coatings on steel during salt spray test.

After 24 h of testing, the three coatings show a greater corrosion resistance than that of bare steel. However, at this time, some pitting is observed in the spray-coated samples with NPs.

At 48 h, in the polymer-based samples (OPSZ:NPs 100:0), salt is deposited on the coatings, although they still resist corrosion. No salt is observed on the coatings that included nanoparticles.

Regarding the samples with the integrated nanoparticles deposited via dip coating, due to their water-repellent character, water deposition is notably reduced in comparison to the control sample. These samples have a greater homogeneity of their finish and, due to this, show a greater resistance to corrosion.

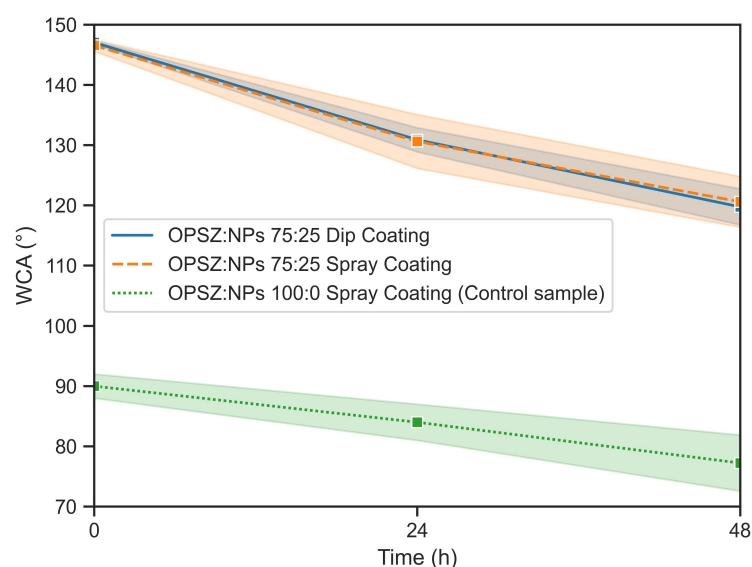


Figure 9. Contact angle measurements versus salt spray test time (shadowed area corresponds to the standard deviation).

On the contrary, in the sprayed coatings (the OPZS:NPs 75:25 spray coating), it can be seen how pitting corrosion begins to appear due to possible imperfections in the finish produced during the spraying process.

Water penetration could not be directly observed in the experiments, but the corrosion in the 75:25 spray-coated sample may be due to the penetration of water through the discontinuities of the surface finish, causing the pitting corrosion phenomenon to take place [37]. Although the control sample is not hydrophobic and droplets of salty water are deposited on the surface, the surface finish is of a higher quality, thus having a lower degree of water penetration, which prevents corrosive species from reaching the metal surface [38]. The defects in the nanocomposite coating deposited via spraying affect the protective function of the coating, which is favorable for the penetration of corrosive media into the film.

The evolution of the contact angle shows a reduction in hydrophobicity over time. However, the values of the WCA obtained for the two deposition methods, spray coating and dip coating, show very similar values. This confirms the fact that the degradation of the spray-deposited samples is due to the bad surface finish and not due to the loss of hydrophobicity.

3.4. Artificial Weathering Test Results

The coatings were exposed to artificial weathering during a 120 h cycle with alternate cycles of rain and UV light, and an inspection was carried out every 24 h.

During the test, the evolution of the samples over time was evaluated with a visual inspection (every 24 h), pictures of which are shown in Figure 10. During the inspections, the WCA was also measured, and it is presented in Figure 11.

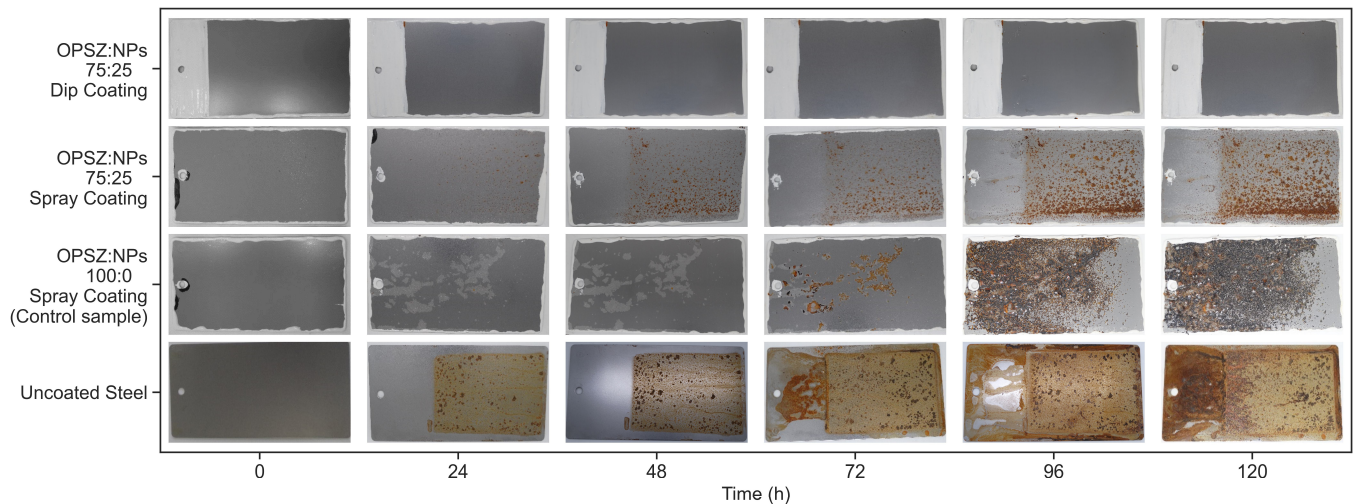


Figure 10. Evolution of coatings on steel during artificial weathering test.

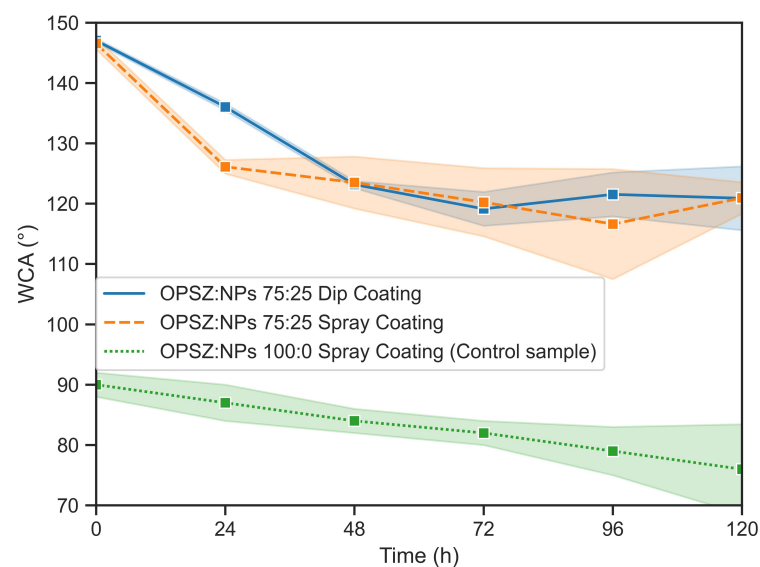


Figure 11. Contact angle measurements versus artificial weathering test time (shadowed area corresponds to the standard deviation).

Before analyzing the results, it should be considered that the artificial weathering test is a severe test, where samples are subjected to thermal shock and UV radiation. In general, both degradation mechanisms promote polymer cracking and color change. In this sense, a clear cracking effect is observed in the control sample (OPSZ:NPs 100:0) following the 24 h exposition. As reported in the literature, numerous cracks appear because of volume shrinkage during the curing process of OPSZs. By adding fillers, this phenomenon is reduced [22].

Otherwise, in the integrated nanoparticle samples, the cracking effect is not detected. This could be explained by the UV light absorption capacity of the SiO₂ nanoparticles and the formation of strong networks between the nanoparticles and polymeric molecules [39].

Regarding the hydrophobic coatings, surface degradation by corrosion is observed in the spray-coated samples (the OPSZ:NPs 75:25 spray coating). Corrosion behavior

similar to that in the salt spray results is observed. The pitting corrosion phenomenon begins to appear early in the control samples and the sprayed coatings with the integrated nanoparticles. However, it is not detected in the dip-coated samples at any time, showing a very good weathering resistance. This corrosion-resistant behavior is very interesting considering the low thickness of the dip-coated samples ($5\ \mu\text{m}$) in comparison to that of the other samples ($>29\ \mu\text{m}$).

Considering the hydrophobic character, it can be observed in Figure 11 that a WCA reduction takes place during the test for both the spray and dip deposition methods, from a highly hydrophobic behavior at $t = 0$ ($\sim 147^\circ$) to a hydrophobic behavior ($\sim 121^\circ$, $t = 120\ \text{h}$). This behavior has already been studied by other authors [15].

3.5. EIS Results

The EIS technique was employed to investigate the anticorrosion performance of the coatings. The Bode modulus and Bode phase as well as the Nyquist plots of the coatings analyzed are depicted in Figures 12–14, respectively. Significant differences in the impedance values between the samples were indeed observed.

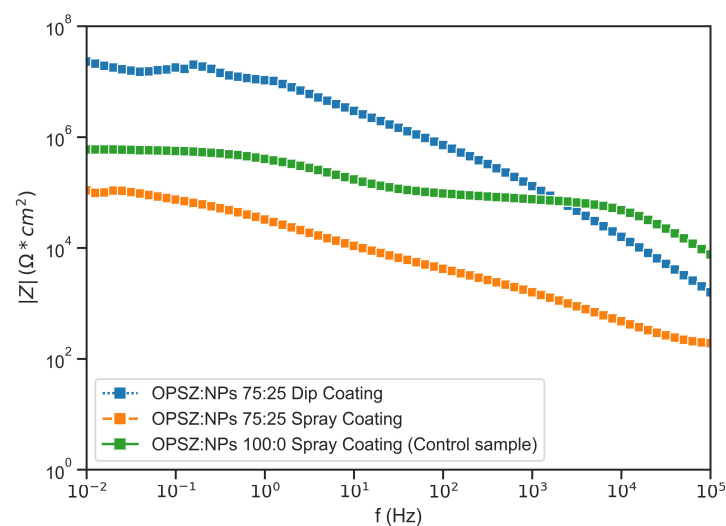


Figure 12. Bode modulus.

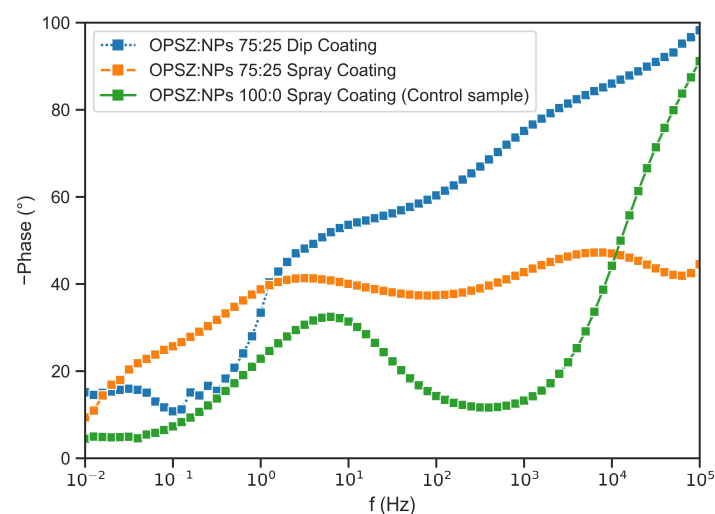


Figure 13. Bode phase.

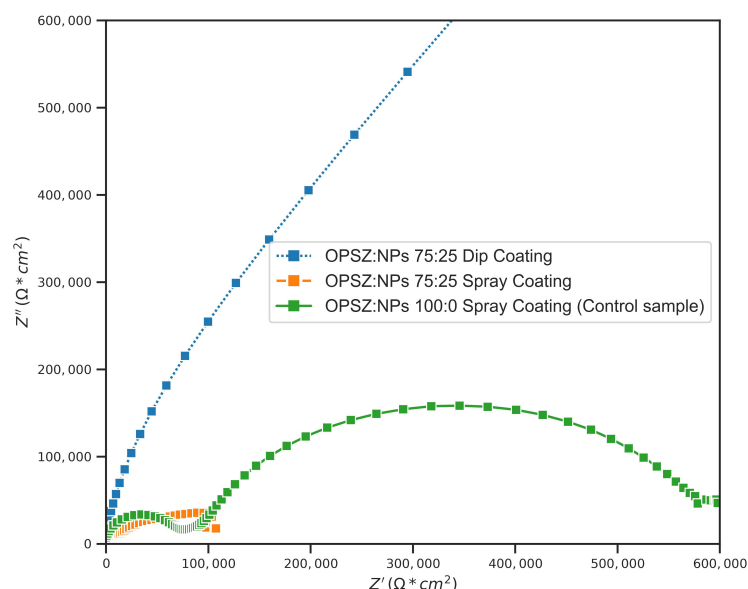


Figure 14. Nyquist plot.

Attending to the Bode modulus plot (Figure 12), the impedance module values, $|Z|$, can be observed at a low frequency, where the highest value corresponds to the dip-coated sample. That is, the dip-coating formulation OPSZ:NPs 75:25 shows the highest impedance modulus in the low-frequency range ($|Z|_{0.01 \text{ Hz}} = 2.2 \cdot 10^7 \Omega \cdot \text{cm}^2$). However, when using the spray-coating technique, the behavior of the system is worse, giving values of the impedance modulus two orders of magnitude lower ($|Z|_{0.01 \text{ Hz}} = 1.1 \cdot 10^5 \Omega \cdot \text{cm}^2$) than those of the dip-coating technique applied to the samples.

The Bode phase plot (Figure 13) properties diminish over time, which means that all the systems are not in the perfect capacitive area whatsoever. This is in accordance with the Nyquist plot (Figure 14), as the coatings treated with the spray-coating technique show an arc far more resistive than that of the dip-coated samples, which is more capacitive and, thus, more likely to reach values of a higher impedance. Additionally, the surfaces of the samples treated using the spray-coating technique show, at high frequencies, a very poor performance on the protective coating side and a very advanced corrosion process at low frequencies due to the existence of pores. This fact allows for the migration of ions from the electrolyte to gain access throughout the net of pores to the metal beneath with considerable ease. The existence of two different arcs depicted by the Nyquist plot explains this electrochemical behavior very well and fits quite well with the visual inspection carried out after the salt spray test (Figure 8).

In addition, considering that the thickness of the dip-coated samples is much smaller than that of the control sample ($5 \mu\text{m}$ vs. $80 \mu\text{m}$), the values of impedance clearly confirm the improvement of the barrier effect promoted by the nanoparticle integration into the polymer.

The EIS analyses are consistent with the results obtained from the salt spray and accelerated weathering tests.

4. Conclusions

The hydrophobic performance of OPSZs combined with SiO_2 nanoparticles was investigated. The environmental degradation of the coatings was evaluated by using different tests, namely, salt spray, accelerated weathering and EIS tests, and the main conclusions are as follows:

1. Hydrophobic surfaces were successfully synthesized using a mixture of OPSZs and hydrophobic SiO_2 nanoparticles. At an NP percentage of 25%, the water contact angle

- of the coatings was 147° in the horizontal plane, which can be considered highly hydrophobic, very close to the superhydrophobic regime.
- Two deposition methods (spray-coating and dip-coating methods) were compared. The results clearly depict a higher level of protection when the dip-coating method was used. The spray-coating method is not appropriate for these types of polymers, causing heterogeneities and defects on the surface finish. The dip-coating method is a facile and low-cost method, and a good surface finish is achieved.
 - The hydrophobic effect favors corrosion resistance, but mainly in a marine environment with atmospheric and splash exposures and not in immersion, where the homogeneity of the coating prevails.
 - The formulation OPSZ:NPs 75:25 deposited using the dip-coating method showed a great corrosion resistance in comparison with that of the other samples, assessed by all the degradation tests. This corrosion-resistant behavior is very interesting considering the low thickness of the dip-coated samples ($5\text{ }\mu\text{m}$) in comparison to that of the other samples ($>29\text{ }\mu\text{m}$).

Author Contributions: Conceptualization, L.P.-G., D.A. and A.Y.; methodology, L.P.-G., D.A., C.M., M.G.-B. and L.S.; software, L.S.; validation, L.P.-G., C.M. and M.G.-B.; formal analysis, L.P.-G., D.A. and A.Y.; investigation, L.P.-G., D.A., C.M., M.G.-B. and L.S.; resources, L.P.-G. and A.Y.; data curation, L.P.-G., D.A. and L.S.; visualization, A.C., L.P.-G. and A.Y.; writing—original draft preparation, L.P.-G., A.C. and A.Y.; writing—review and editing, L.P.-G., A.C. and A.Y.; supervision, L.P.-G., A.C. and A.Y.; project administration, L.P.-G. and A.Y.; funding acquisition, L.P.-G. and A.Y. All authors have read and agreed to the published version of the manuscript.

Funding: This research was funded by the Ministry of Science, Innovation and Universities of Spain, through the Torres Quevedo Program, grant number PTQ2018-009743.

Institutional Review Board Statement: Not applicable.

Informed Consent Statement: Not applicable.

Data Availability Statement: Not applicable.

Acknowledgments: We would like to thank Merck KGaA and specially Ralf Grottenmueller, Juergen Mertes and Christoph Landmann for providing organopolysilazane samples and technical assistance. Their support is greatly appreciated. We would also like to thank Alejandro Cabrera Felipe for his support in the technical discussion of the EIS test results.

Conflicts of Interest: The authors declare no conflict of interest. The funders had no role in the design of the study; in the collection, analyses, or interpretation of data; in the writing of the manuscript; or in the decision to publish the results.

References

- Simpson, J.T.; Hunter, S.R.; Aytug, T. Superhydrophobic Materials and Coatings: A Review. *Rep. Prog. Phys.* **2015**, *78*, 086501. [\[CrossRef\]](#)
- Mohamed, A.M.A.; Abdullah, A.M.; Younan, N.A. Corrosion Behavior of Superhydrophobic Surfaces: A Review. *Arab. J. Chem.* **2015**, *8*, 749–765. [\[CrossRef\]](#)
- Cao, L.; Lu, X.; Pu, F.; Yin, X.; Xia, Y.; Huang, W.; Li, Z. Facile Fabrication of Superhydrophobic Bi/Bi₂O₃ Surfaces with Hierarchical Micro-Nanostructures by Electroless Deposition or Electrodeposition. *Appl. Surf. Sci.* **2014**, *288*, 558–563. [\[CrossRef\]](#)
- Wu, L.-K.; Hu, J.-M.; Zhang, J.-Q. One Step Sol–Gel Electrochemistry for the Fabrication of Superhydrophobic Surfaces. *J. Mater. Chem. A Mater.* **2013**, *1*, 14471. [\[CrossRef\]](#)
- Wu, X.; Fu, Q.; Kumar, D.; Ho, J.W.C.; Kanhere, P.; Zhou, H.; Chen, Z. Mechanically Robust Superhydrophobic and Superoleophobic Coatings Derived by Sol–Gel Method. *Mater. Des.* **2016**, *89*, 1302–1309. [\[CrossRef\]](#)
- Barshilia, H.C.; Ananth, A.; Gupta, N.; Anandan, C. Superhydrophobic Nanostructured Kapton® Surfaces Fabricated through Ar+O₂ Plasma Treatment: Effects of Different Environments on Wetting Behaviour. *Appl. Surf. Sci.* **2013**, *268*, 464–471. [\[CrossRef\]](#)
- Rezaei, S.; Manoucheri, I.; Moradian, R.; Pourabbas, B. One-Step Chemical Vapor Deposition and Modification of Silica Nanoparticles at the Lowest Possible Temperature and Superhydrophobic Surface Fabrication. *Chem. Eng. J.* **2014**, *252*, 11–16. [\[CrossRef\]](#)

8. Blinov, A.V.; Kostyukov, D.A.; Yasnaya, M.A.; Zvada, P.A.; Arefeva, L.P.; Varavka, V.N.; Zvezdilin, R.A.; Kravtsov, A.A.; Maglakelidze, D.G.; Golik, A.B.; et al. Oxide Nanostructured Coating for Power Lines with Anti-Icing Effect. *Coatings* **2022**, *12*, 1346. [\[CrossRef\]](#)
9. Blinov, A.V.; Nagdalian, A.A.; Arefeva, L.P.; Varavka, V.N.; Kudryakov, O.V.; Gvozdenko, A.A.; Golik, A.B.; Blinova, A.A.; Maglakelidze, D.G.; Filippov, D.D.; et al. Nanoscale Composite Protective Preparation for Cars Paint and Varnish Coatings. *Coatings* **2022**, *12*, 1267. [\[CrossRef\]](#)
10. Bai, Y.; Zhang, H.; Shao, Y.; Zhang, H.; Zhu, J. Recent Progresses of Superhydrophobic Coatings in Different Application Fields: An Overview. *Coatings* **2021**, *11*, 116. [\[CrossRef\]](#)
11. Millionis, A.; Loth, E.; Bayer, I.S. Recent Advances in the Mechanical Durability of Superhydrophobic Materials. *Adv. Colloid Interface Sci.* **2016**, *229*, 57–79. [\[CrossRef\]](#)
12. Zhi, J.-H.; Zhang, L.-Z.; Yan, Y.; Zhu, J. Mechanical Durability of Superhydrophobic Surfaces: The Role of Surface Modification Technologies. *Appl. Surf. Sci.* **2017**, *392*, 286–296. [\[CrossRef\]](#)
13. Montemor, M.F. Functional and Smart Coatings for Corrosion Protection: A Review of Recent Advances. *Surf. Coat. Technol.* **2014**, *258*, 17–37. [\[CrossRef\]](#)
14. Carreño, F.; Gude, M.R.; Calvo, S.; Rodríguez de la Fuente, O.; Carmona, N. Synthesis and Characterization of Superhydrophobic Surfaces Prepared from Silica and Alumina Nanoparticles on a Polyurethane Polymer Matrix. *Prog. Org. Coat.* **2019**, *135*, 205–212. [\[CrossRef\]](#)
15. Zhi, D.; Lu, Y.; Sathasivam, S.; Parkin, I.P.; Zhang, X. Large-Scale Fabrication of Translucent and Repairable Superhydrophobic Spray Coatings with Remarkable Mechanical, Chemical Durability and UV Resistance. *J. Mater. Chem. A Mater.* **2017**, *5*, 10622–10631. [\[CrossRef\]](#)
16. Xu, L.; He, J. Fabrication of Highly Transparent Superhydrophobic Coatings from Hollow Silica Nanoparticles. *Langmuir* **2012**, *28*, 7512–7518. [\[CrossRef\]](#) [\[PubMed\]](#)
17. Chen, Z.; Li, G.; Wang, L.; Lin, Y.; Zhou, W. A Strategy for Constructing Superhydrophobic Multilayer Coatings with Self-Cleaning Properties and Mechanical Durability Based on the Anchoring Effect of Organopolysilazane. *Mater. Des.* **2018**, *141*, 37–47. [\[CrossRef\]](#)
18. Kroke, E.; Li, Y.-L.; Konetschny, C.; Lecomte, E.; Fasel, C.; Riedel, R. Silazane Derived Ceramics and Related Materials. *Mater. Sci. Eng. R Rep.* **2000**, *26*, 97–199. [\[CrossRef\]](#)
19. Bhandavat, R.; Feldman, A.; Cromer, C.; Lehman, J.; Singh, G. Very High Laser-Damage Threshold of Polymer-Derived Si(B)CN-Carbon Nanotube Composite Coatings. *ACS Appl. Mater. Interfaces* **2013**, *5*, 2354–2359. [\[CrossRef\]](#)
20. Li, D.; Guo, P.; Guzi de Moraes, E.; Wan, W.; Zou, J.; Colombo, P.; Shen, Z. Structural Study of Disordered SiC Nanowires by Three-Dimensional Rotation Electron Diffraction. *Mater. Res. Express* **2014**, *1*, 045023. [\[CrossRef\]](#)
21. Fedel, M.; Rodríguez Gómez, F.J.; Rossi, S.; Deflorian, F. Characterization of Polyorganosilazane-Derived Hybrid Coatings for the Corrosion Protection of Mild Steel in Chloride Solution. *Coatings* **2019**, *9*, 680. [\[CrossRef\]](#)
22. Wang, G.; Wang, J.; Wang, J.; Chi, Z.; Zhang, G.; Zhou, Z.; Feng, Z.; Xiong, Y. A Sinter Visualization Device for Observing the Relationship Between Fillers and Porosity of Precursor-Derived Ceramic Coatings. *Coatings* **2020**, *10*, 552. [\[CrossRef\]](#)
23. Riedel, R.; Mera, G.; Hauser, R.; Klonczynski, A. Silicon-Based Polymer-Derived Ceramics: Synthesis Properties and Applications—A Review. *J. Ceram. Soc. Jpn.* **2006**, *114*, 425–444. [\[CrossRef\]](#)
24. Hu, L.; Zhang, L.; Wang, D.; Lin, X.; Chen, Y. Fabrication of Biomimetic Superhydrophobic Surface Based on Nanosecond Laser-Treated Titanium Alloy Surface and Organic Polysilazane Composite Coating. *Colloids Surf. A Physicochem. Eng. Asp.* **2018**, *555*, 515–524. [\[CrossRef\]](#)
25. Huang, X.; Wang, D.; Hu, L.; Song, J.; Chen, Y. Preparation of a Novel Antibacterial Coating Precursor and Its Antibacterial Mechanism. *Appl. Surf. Sci.* **2019**, *465*, 478–485. [\[CrossRef\]](#)
26. Rossi, S.; Deflorian, F.; Fedel, M. Polysilazane-Based Coatings: Corrosion Protection and Anti-Graffiti Properties. *Surf. Eng.* **2019**, *35*, 343–350. [\[CrossRef\]](#)
27. Coan, T.; Barroso, G.S.; Machado, R.A.F.; de Souza, F.S.; Spinelli, A.; Motz, G. A Novel Organic-Inorganic PMMA/Polysilazane Hybrid Polymer for Corrosion Protection. *Prog. Org. Coat.* **2015**, *89*, 220–230. [\[CrossRef\]](#)
28. Available online: <https://www.geogebra.org/classic> (accessed on 23 December 2021).
29. Montemor, M.F. *Smart Composite Coatings and Membranes*; Elsevier: Amsterdam, The Netherlands, 2016; ISBN 9781782422839.
30. ISO 16773-4:2017; Electrochemical Impedance Spectroscopy (EIS) on Coated and Uncoated Metallic Specimens—Part 4: Examples of Spectra of Polymer-Coated and Uncoated Specimens. International Organization for Standardization: Geneva, Switzerland, 2017.
31. Dickie, R.A.; Floyd, F.L. Polymeric Materials for Corrosion Control: An Overview. In *Polymeric Materials for Corrosion Control*; American Chemical Society: Washington, WA, USA, 1986; pp. 1–16.
32. Cai, C.; Sang, N.; Teng, S.; Shen, Z.; Guo, J.; Zhao, X.; Guo, Z. Superhydrophobic Surface Fabricated by Spraying Hydrophobic R974 Nanoparticles and the Drag Reduction in Water. *Surf. Coat. Technol.* **2016**, *307*, 366–373. [\[CrossRef\]](#)
33. Karmouch, R.; Ross, G.G. Superhydrophobic Wind Turbine Blade Surfaces Obtained by a Simple Deposition of Silica Nanoparticles Embedded in Epoxy. *Appl. Surf. Sci.* **2010**, *257*, 665–669. [\[CrossRef\]](#)
34. Manoudis, P.N.; Karapanagiotis, I.; Tsakalof, A.; Zuburtikudis, I.; Panayiotou, C. Superhydrophobic Composite Films Produced on Various Substrates. *Langmuir* **2008**, *24*, 11225–11232. [\[CrossRef\]](#)

35. Chatzigrigoriou, A.; Karapanagiotis, I.; Poullos, I. Superhydrophobic Coatings Based on Siloxane Resin and Calcium Hydroxide Nanoparticles for Marble Protection. *Coatings* **2020**, *10*, 334. [[CrossRef](#)]
36. Chavez, R.; Ionescu, E.; Balan, C.; Fasel, C.; Riedel, R. Effect of Ambient Atmosphere on Crosslinking of Polysilazanes. *J. Appl. Polym. Sci.* **2011**, *119*, 794–802. [[CrossRef](#)]
37. Barkhudarov, P.M.; Shah, P.B.; Watkins, E.B.; Doshi, D.A.; Brinker, C.J.; Majewski, J. Corrosion Inhibition Using Superhydrophobic Films. *Corros. Sci.* **2008**, *50*, 897–902. [[CrossRef](#)]
38. Ou, J.; Liu, M.; Li, W.; Wang, F.; Xue, M.; Li, C. Corrosion Behavior of Superhydrophobic Surfaces of Ti Alloys in NaCl Solutions. *Appl. Surf. Sci.* **2012**, *258*, 4724–4728. [[CrossRef](#)]
39. Yedra, Á.; Gutiérrez-Somavilla, G.; Manteca-Martínez, C.; González-Barriuso, M.; Soriano, L. Conductive Paints Development through Nanotechnology. *Prog. Org. Coat.* **2016**, *95*, 85–90. [[CrossRef](#)]

Disclaimer/Publisher's Note: The statements, opinions and data contained in all publications are solely those of the individual author(s) and contributor(s) and not of MDPI and/or the editor(s). MDPI and/or the editor(s) disclaim responsibility for any injury to people or property resulting from any ideas, methods, instructions or products referred to in the content.